Journal of Membrane Science 661 (2022) 120794

Contents lists available at ScienceDirect

Journal of Membrane Science

journal homepage: www.elsevier.com/locate/memsci

Thermo-responsive graft copolymer PSf-g-PNIPM: Reducing the structure parameter via morphology control of forward osmosis membrane substrates

Hasan Salehi [a], Alireza Shakeri [a,*], Rob G.H. Lammertink [b,**]

[a] School of Chemistry, College of Science, University of Tehran, P.O. Box 14155-6619, Tehran, Iran
[b] Soft Matter, Fluidics and Interfaces, Membrane Science and Technology, MESA+ Research Institute, University of Twente, P.O. Box 217, NL-7500 AE Enschede, the Netherlands

ARTICLE INFO

Keywords:
Amphiphilic graft copolymer
Forward osmosis
Substrate
Thermo-responsive

ABSTRACT

An amphiphilic graft copolymer, consisting of a polysulfone (PSf) main chain and poly(n-isopropylacrylamide) (PNIPM) grafts, was synthesized via a combination of atom transfer radical polymerization and click chemistry. The copolymer's structure characteristics (PNIPM length and content) substantially impacts membrane morphology and performance, and were optimized firstly. The resulting copolymer PSf-g-PNIPM with the best characteristics was used as an additive in the fabrication of PSf porous substrates by phase inversion. The effect of the graft copolymer on the physicochemical characteristics and performance of PSf substrate was thoroughly studied. The pure water permeability displays a temperature dependency for PSf substrates with 20 wt% PSf-g-PNIPM, with the maximum above the LCST of the PNIPM side chains. Thin film composite membranes formed on these substrates via interfacial polymerization show a significantly improved water flux during forward osmosis operation. The morphology and performance of the PSf-g-PNIPM modified substrate can be further tuned by the casting medium temperature. Membranes formed below the LCST show higher porosity and water flux.

1. Introduction

Freshwater shortage is a serious challenge that worsens by climate change, increasing population and urbanization [1]. Hence, advanced technologies are required to overcome this issue. Recently, forward osmosis (FO) as an energy-efficient membrane technology has received increased attention [2,3]. FO uses natural osmotic pressure to drive the separation process, which leads to lower membrane fouling, equipment cost, and energy consumption than conventional pressure driven membrane process [4–8]. However, internal concentration polarization (ICP) is still a critical challenge for FO processes [9,10]. ICP mostly happens within the substrate of thin film composite (TFC) membranes and lowers the overall FO membrane performance via reducing the local osmotic pressure difference across the membrane [6]. The intensity of ICP can be estimated by the structural parameter, S (μm), which is defined as:

$$S = \frac{l \times \tau}{\varepsilon}$$

Where ε, τ, and l represent the porosity, tortuosity, and thickness of the substrate. A smaller S parameter directs lower ICP effects [11,12]. To lower the S parameter, the ideal substrate should have high porosity, minimal tortuosity, and a low thickness [13]. Huge research efforts have been devoted to reducing ICP and its destructive effects on the FO process, including embedding nanomaterials to enhance water transport and blending hydrophilic polymers to produce a highly hydrophilic and porous structure [14–17]. These modified substrates make TFC membranes more permeable. Using these strategies, different substrates for TFC membranes have been fabricated from hydrophilic polymers such as polyacrylic acid/polyethersulfone (PES) [18], sulfonated polysulphone (SPSf)/polyvinyl chloride (PVC) [5], polyvinyl benzimidazole/PVC [19], or inorganic nanomaterials such as layered double hydroxide/PSf [20], halloysite nanotube/PSf [21] and zeolite/PES [22]. Some reported membrane formulations still face challenges due to the incompatibility between the hydrophilic materials and the hydrophobic support layer polymers [23]. This issue can be solve using amphiphilic graft copolymers, which possess both hydrophilic and hydrophobic segments. The hydrophilic segments present the desired hydrophilicity, while the hydrophobic segments improve the support layer's compatibility and stability [23–25].

The current work aims to prepare a hydrophilic and porous substrate

* Corresponding author.
** Corresponding author.
E-mail addresses: alireza.shakeri@ut.ac.ir (A. Shakeri), r.g.h.lammertink@utwente.nl (R.G.H. Lammertink).

https://doi.org/10.1016/j.memsci.2022.120794
Received 17 March 2022; Received in revised form 25 June 2022; Accepted 3 July 2022
Available online 5 August 2022

Abbreviations

AFM	Atomic force microscopy
ATR-FTIR	Attenuated total reflectance Fourier transform infrared
ATRP	Atom transfer radical polymerization
CPSf	Chloromethylated polysulfone
DI	Deionized
DP	Degree of polymerization
DS	Draw solution
FO	Forward osmosis
FS	Feed solution
ICP	Internal concentration polymerization
IP	Interfacial polymerization
LCST	Lower critical solution temperature
MPD	m-phenylenediamine
NaCl	sodium chloride
NMP	N-methyl pyrrolidone
PA	Polyamide
NIPM	n-isopropylacrylamide
NIPS	Non-solvent-induced phase separation
n-ST	Non-solvent temperature
PBiB	Propargyl 2-bromoisobutyrate
PDETA	N,N,N′,N’,N″-pentamethyl diethylene triamine
PES	Polyethersulfone
PSf	Polysulfone
PVC	Polyvinyl chloride
PWP	Pure water permeability
RO	Reverse osmosis
SEM	Scan electron microscopy
TFC	Thin-film composite
TGA	Thermogravimetric analysis
THF	Tetrahydrofuran
TMC	1,3,5-trimesoyl chloride
WCA	Water contact angle

for TFC-FO membranes using an amphiphilic copolymer additive strategy. Given that graft copolymers with a large excluded volume should segregate more easily than a block or random copolymer [26], we chose polysulfone-graft-poly(n-isopropylacrylamide) (PSf-g-PNIPM) as an amphiphilic graft copolymer to modify PSf substrates. This graft copolymer was synthesized by atom transfer radical polymerization (ATRP) of NIPAM monomer using an alkyne functionalized propargyl 2-bromoisobutyrate (PBiB) initiator. The alkyne terminated PNIPM was grafted on the azide-functionalized PSf polymer backbone by click reaction. PSf was chosen as the main polymer due to its miscibility and compatibility with the substrate base polymer, which should increase the final substrate's stability. PNIPM was also used as a graft because the stretching/coiling conformation changes of PNIPM chains around their lower critical solution temperature (LCST, ~32 °C) providing additional control of the membrane morphology following phase inversion. The sublayer was fabricated by non-solvent-induced phase separation (NIPS) of PSf/PSf-g-NIPAM solution blends. Interfacial polymerization (IP) was performed on top of these supports to form a thin polyamide (PA) layer. The effect of the PSf/PSf-g-NIPAM mass ratio on the hydrophilicity, porosity and separation performance of the resulting TFC-FO membranes was investigated.

2. Experimental

2.1. Materials

Chloromethylated PSf (CPSf) and PSf-N_3 were synthesized by chloromethylation and following azide functionalization of PSf (Ultrason S6010, BASF), based on Ref. [27]. N-methyl-2-pyrrolidone (Merck, NMP, 98%) was used as PSf and graft copolymers solvent. N-Isopropylacrylamide (Sigma Aldrich, NIPM, 98%), N,N,N′,N’,N″-pentamethyl diethylene triamine (Merck, PMDETA, 98%), copper (I) chloride (Sigma Aldrich, 99%), tetrahydrofuran (Merck, THF, 99%), diethyl ether (Merck, 99%), and 2-propanol (Merck, 99%) were used for the synthesis of PNIPM via ATRP reaction. PBiB as alkyne functionalized ATRP initiator was synthesized similarly to our previously reported works [27]. NaCl (Iran Mineral Salt Company) was used as draw agent in FO and feed solution in RO tests. IP reaction was done using trimesoyl chloride (Merck, TMC, 98%) and m-phenylenediamine (Merck, MPD, > 99%) monomers.

2.2. Synthesis of alkyne-terminated PNIPM homopolymer (alkynyl-PNIPM)

The typical synthesis of PNIPM homopolymer capped with an alkyne group was performed as follows. To a 25 mL round bottom flask, NIPM (2 g, 18 mmol), PMDETA (0.03 g, 0.18 mmol) and PBiB (0.04 g, 0.18 mmol) were dissolved in 12 mL of 2-propanol. Under a nitrogen atmosphere, CuCl (0.009 g, 0.09 mmol) was added and the mixture was stirred for a specific time (8, 12, 16 h) at 80 °C. The reaction was then diluted with THF and the mixture was passed through an alumina column to remove the catalyst. After most of the THF was removed using rotary evaporation, the residual was precipitated in an excess of diethyl ether. The precipitate was isolated by filtration and dried under a vacuum. The as-synthesized polymers were denoted as PNIPM-8, PNIPM-12, PNIPM-16 based on the ATRP reaction time. The degree of polymerization (DP) was obtained by ^{1}H NMR analysis, and the results are shown in Table 1.

2.3. Synthesis of the PSf-g-PNIPM graft copolymers

Graft copolymers with different side-chain lengths and graft ratios were synthesized via the click reaction method described in another research [23,27]. The characteristics of synthesized graft copolymers is summarized in Table 1. The as-synthesized graft copolymers were denoted as PSf-g-PNIPM^t_x (t represent the ATRP reaction time and x represent the PSf/PNIPM ratio).

2.4. Preparation of the porous membrane substrates

The membrane substrates were prepared using the NIPS technique. Typically, PSf and PSf-g-PNIPM (15 wt%) were dissolved in the NMP (85 wt%) by stirring at 50 °C for 8 h and then degassed at room temperature. The PSf/PSf-g-PNIPM solution was then poured onto a clean glass plate and spread using a film applicator with a gate height of 100 μm. The glass plate was immediately immersed into the non-solvent (DI water) coagulation bath to initiate phase separation. The fabricated substrates were then kept in DI water to remove the residual solvent while water was changed daily. The compositions of substrates are tabulated in Table 2.

Table 1
Characteristics of synthesized PSf-g-PNIPM.

Graft copolymer	DP of PNIPM	PNIPM content (wt.%)
PSf-g-PNIPM$^{12}_1$	52	50
PSf-g-PNIPM$^{12}_2$	52	33
PSf-g-PNIPM$^{12}_3$	52	25
PSf-g-PNIPM$^{12}_4$	52	20
PSf-g-PNIPM$^{8}_3$	28	25
PSf-g-PNIPM$^{16}_3$	72	25

Table 2
Composition of fabricated substrates and resulting TFCs.

Substrate	PSf-g-PNIPM type	Total polymer (15 wt%)		Resultant TFC
		PSf-g-PNIPM	PSf	
M.0	–	–	100	TFC-M.0
M.n5	PSf-g-PNIPM$_3^{12}$	5	95	TFC-M.n5
M.n10	PSf-g-PNIPM$_3^{12}$	10	90	TFC-M.n10
M.n15	PSf-g-PNIPM$_3^{12}$	15	85	TFC-M.n15
M.n20	PSf-g-PNIPM$_3^{12}$	20	80	TFC-M.n20
M.n25	PSf-g-PNIPM$_3^{12}$	25	75	TFC-M.n25
M.s20	PSf-g-PNIPM$_3^{8}$	20	80	TFC-M.s20
M.l20	PSf-g-PNIPM$_3^{16}$	20	80	TFC-M.l20
M.d20	PSf-g-PNIPM$_4^{12}$	20	80	TFC-M.d20

2.5. Preparation of thin-film composite membranes

TFC membranes with different sublayers were fabricated by IP reaction between TMC-organic and MPD-aqueous solutions at the top of the porous membrane substrates. In brief, 2.0 wt% MPD aqueous solution was soaked into the PSf/PSf-PNIPM substrate for 120 s. Then the excess monomer solution was removed using an air knife. To initiate polymerization, the TMC-organic solution (0.1 wt% in n-hexane) was gently poured on the MPD saturated surface and removed after 90 s. Next, the membranes were thermally cured in an oven at 60 °C for 1 min. Finally, they were rinsed thoroughly with water and stored in DI water.

2.6. Characterization of copolymer, substrate and composite membranes

Thermogravimetric analysis (TGA, Q5000IR TA instrument, USA) and ^{1}H NMR spectrometry (Bruker Co., Germany 500 MHz) were used to record the copolymers' thermogram and ^{1}H NMR spectra, respectively. The functional groups of the synthesized polymers and prepared membranes were further examined by ATR-FTIR (Bruker, Equinox 55). The surface wettability and roughness of the membranes were investigated by contact angle analysis (Dataphysics, OCA 15 plus) and atomic force microscopy (AFM, ENTEGRA AFMNT- MDT), respectively. Membrane cross-section, bottom and top surface morphology were characterized by SEM (Tescan, VEGA). The porosity (ε) of the support layers was measured based on the weights of imbibed water in the pores of substrates by equation (1).

$$\varepsilon = \frac{(m_1 - m_2)/\rho_W}{(m_1 - m_2)/\rho_W + m_2/\rho_P} \tag{1}$$

where m_1 and m_2 represent the wet and dry mass of the support layer, respectively, and ρ_w and ρ_p are the density of water and polymer, respectively.

The pure water permeability (PWP, LMHbar^{-1}) of the support layers was measured in a cross-flow filtration setup based on the volume of permeate (V) over the test time (Δt). The effective membrane area (A_m) and operating pressure (P) were 4.9 cm^2 and 2 bar, respectively.

$$PWP = \frac{V}{A_m \times \Delta t \times P} \tag{2}$$

The mean pore size (r_m) of the support layers was calculated based on the porosity and PWP data according to the Gerout-Elford-Ferry equation [28]:

$$r_m = \sqrt{\frac{(2.9 - 1.75\varepsilon) \times 8Q\mu z}{\varepsilon \times A_m \times \Delta P}} \tag{3}$$

where z, μ and Q represent the membrane thickness (μm), water viscosity (Pa.s) and water flow (m^{3}s^{-1}), respectively.

The intrinsic separation properties of the membrane were examined in a dead-end RO cell. Salt rejection (R_s) and water permeability (A) were measured at 5 bar (ΔP) with 1000 ppm NaCl (C_f) in DI water as feed solution. The salt permeability coefficient (B) was calculated according to equation (6). All the tests were carried out using a membrane with a surface area of 3.1 cm^2 (A_m) at 25 °C.

$$J = \frac{\Delta V}{A_m \times \Delta t \times \Delta P} \tag{4}$$

$$R_s = \left(1 - \frac{C_p}{C_f}\right) \times 100 \tag{5}$$

$$\frac{1 - R_s}{R_s} = \frac{B}{A(\Delta P - \Delta \pi)} \tag{6}$$

The osmosis performance of the modified membranes was measured using a bench-scale FO setup. The measurements used DI water as feed solution, 1 M NaCl as draw solution, and a crossflow velocity of 0.34 m/s for both feed and draw solutions. The water flux (J_w, LMH) and reverse salt flux (J_s, gMH) were calculated by measuring the volume of permeate water (ΔV) and mass of permeated salt (Δm) over a specific test time (Δt) and membrane surface area (A_m) based on equations (7) and (8). The water amount and conductivity change were monitored using a balance and conductivity meter, respectively.

$$J_w = \frac{\Delta V}{A_m \Delta t} \tag{7}$$

$$J_S = \frac{\Delta m}{A_m \Delta t} \tag{8}$$

The structure parameter S for each substrate was calculated according to equation (9):

$$S = \frac{D_s}{J_w} ln \frac{A\pi_D + B}{A\pi_F + J_w + B} \tag{9}$$

where π_F and π_D are the osmotic pressure at the feed and draw side, and D_s is the solute diffusion coefficient.

3. Results and discussion

The effect of graft copolymer parameters on membrane performance. The length and content of the PNIPM in graft copolymer are important parameters controlling the morphology and performance of the modified substrates. Based on this fact, we synthesized graft copolymers with three of different graft lengths and four of different graft ratios (characterization results with details are provided in Supporting information). Then, we examined the effect of PSf-g-PNIPM copolymer composition on the characteristics and performance of substrates and resultant TFC membranes to find the optimal graft copolymer. Fig. 1 shows the water and reverse salt fluxes of the control and modified TFC membranes. Overall, the modified TFC-FO membranes with a PSf/PSf-g-PNIPM substrate have better performance than TFC membrane with a pristine PSf substrate. The water flux increased from 20.8 for TFC-s20 to 28.4 LMH for TFC-n20, which is accompanied by an increase in DP of PNIPM from 28 to 52. However, a further rise in DP (72) led to a decline in water flux of TFC-M.l20 to 21.6 LMH. Moreover, the water flux significantly decreases with the decrease in graft content from 25 to 20 wt% in the PSf-g-PNIPM copolymer.

To relate the copolymer structure parameters to the FO performance, the physicochemical characteristics and morphology of the modified sublayer were studied and compared with control PSf. The data summarized in Table 3 reveal that all modified sublayers have a slightly higher porosity but significantly enhanced PWP, suggesting larger pore diameters than those of the control PSf sublayer. These improvements in modified sublayer characteristics are believed to be due to the pore-forming ability of amphiphilic graft copolymers [24,29]. The graft copolymer type further influences the performance. It could be easily found that all of these characteristics decreased as the graft ratio decreased from 25 wt% in M.n20 to 20 wt% in M.d20. The major reason

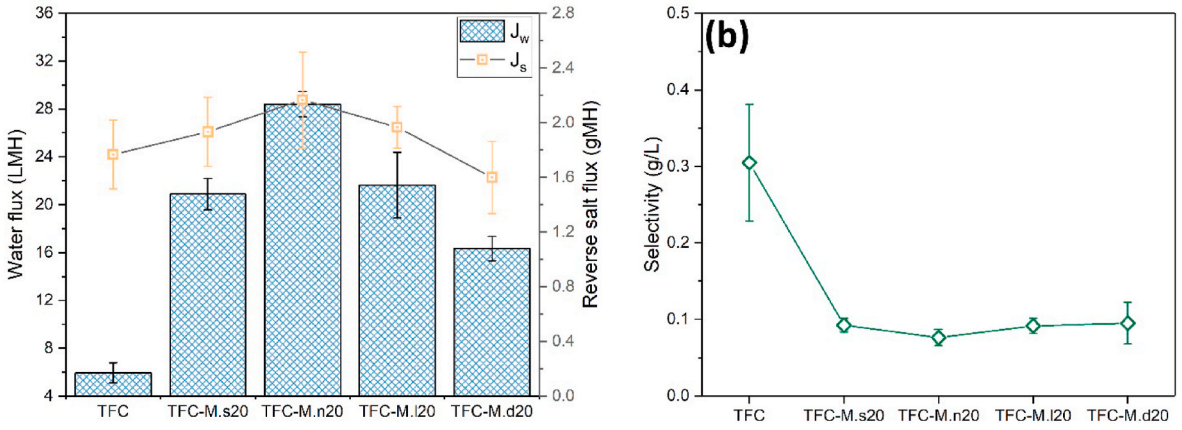

Fig. 1. FO performance of TFC membranes with different substrates.

Table 3
The effect of copolymer structure parameter on characteristics of modified substrates.

Membrane	Substrate			
	Porosity (%)	WCA (°)	PWP (LMH/bar)	Pore size (nm)
M.0	77.3 ± 1.2	80.1 ± 1.7	79.7 ± 11.9	13.7
M.s20	79.5 ± 1.1	68.2 ± 0.8	287 ± 9.8	24.1
M.n20	84.1 ± 0.2	69.3 ± 1.3	345.3 ± 14.6	26.9
M.l20	82.1 ± 0.8	70.5 ± 1.4	304 ± 13.2	25.4
M.d20	78.8 ± 0.7	73.1 ± 0.9	215 ± 11.3	22.2

for these phenomenon's could be attributed to the low hydrophilic side chain content in copolymer structure. The reduced water flux in the TFC-M.d20 membrane can be attributed to the low porosity and hydrophilicity in its sublayer, which increases the S parameter and thus enhances ICP. The porosity and surface pore diameter increase with rise in DP of PNIPM from 28 in M.s20 to 52 in M.n20. Therefore, the improved porosity in the M.n20 sublayer are responsible for enhanced water flux in the TFC-M.n20 membrane. However, a further increase in DP of PNIPM cannot enhance the porosity. In addition, the higher hydrophilicity of modified membranes may be affected the performance-enhancing of the TFC-FO membrane.

The morphology of the modified substrates was also characterized by SEM images (Fig. 2). As can be seen there is no distinct difference in cross section and top surface morphology with DP of PNIPM. However, PNIPM content has a notable influence on the substrate cross-section morphology. Compared to the M.n20, a short finger-like morphology was observed for the M.d20, which might be largely contributed to the low content of hydrophilic side chain, although there is no clear change in the top surface in comparison to the M.n20.

One point that should be noted is that all modified membranes exhibited better selectivity than the TFC membrane (Fig. 1). As shown in Fig. 2, the uniform PA thin film formed onto such modified sublayers could explain enhanced selectivity. It is reasonable to conclude that support layer and PA thin film characteristics could improve by amphiphilic graft copolymer additive strategy. Therefore, both the length and content of side chains can affect the TFC membrane performance in FO process. Based on both support layer characteristics and FO performance, it seems PNIPM with DP of 52 and content of 25 wt% is appropriate for the sublayer modification in the following studies.

Characteristics and performances of the sublayers. The modified sublayers were extensively characterized to study the copolymer blending effect on the sublayer properties and performance. The presence of graft copolymer in the sublayers matrix was proved using ATR-FTIR. Fig. 3 presents the ATR-FTIR spectra of both control and modified sublayers. The modified sublayers exhibited two new peaks at 1650 and 1550 cm^{-1}. These peaks, which are not present in the spectrum of the control PSf sublayer, are due to the –CO-NH stretching vibration of PNIPM [30].

Table 4 summarizes some properties of the modified sublayers with various PSf-g-PNIPM content. The modified sublayer's hydrophilicity was measured based on WCA analysis. The M.n25 presents a reduced WCA of 64.1° compared to 80.1° for the PSf control membrane. This improvement likely results from the presence of hydrophilic PNIPM at the membrane surface. The copolymer blending increased the porosity of the modified sublayers to 84.1% for M.n20, which is significantly higher than the control membrane porosity (77.3%). Also, the sublayers' mean pore size, an important feature in controlling the PA layer morphology, increased to 26.3 nm upon blending with 20 wt% of the copolymer. This value was considerably larger than the corresponding value of 13.7 nm for the control PSf sublayer. Such observations are consistent with previous reports, where the hydrophilic additive increases the substrate porosity and surface pore size [5,14,31]. The improved mean surface pore size and porosity of the prepared substrate have been attributed to increasing the hydrophilicity of casting solution with a slower exchange rate between solvent and non-solvent [32].

The effect of graft copolymer addition on the PWP of modified substrates was also investigated using a cross-flow UF setup. The control PSf substrate, due to its lower hydrophilicity, surface pore size and porosity, shows the lowest PWP of 79.7 LMH/bar. The PWP of copolymer blended substrates considerably improved up to 345.3 LMH/bar for M.n20. This enhancement should come from the enhanced hydrophilicity and the reduced resistance due to their large surface pore size and high porosity. The slight decline in the PWP of M-n25 is probably resulting from the denser substrate surface with slightly lower porosity.

Generally, the pore surface composition and pore size distribution of the sublayer significantly control the permeation through the membrane. Temperature dependent PWP of M.0 and M.n20 membranes were measured using DI water at different temperatures, as PNIMP is known for its temperature dependent conformation. Giving Hagen-Poiseuolle's law, the viscosity, and consequently the water permeability through the porous membrane are dependent on permeate temperature [33]. The measured water permeability was corrected for this to eliminate the effect of water viscosity on PWP [34,35].

The control M.0, shows only a slight change as the temperature rises.

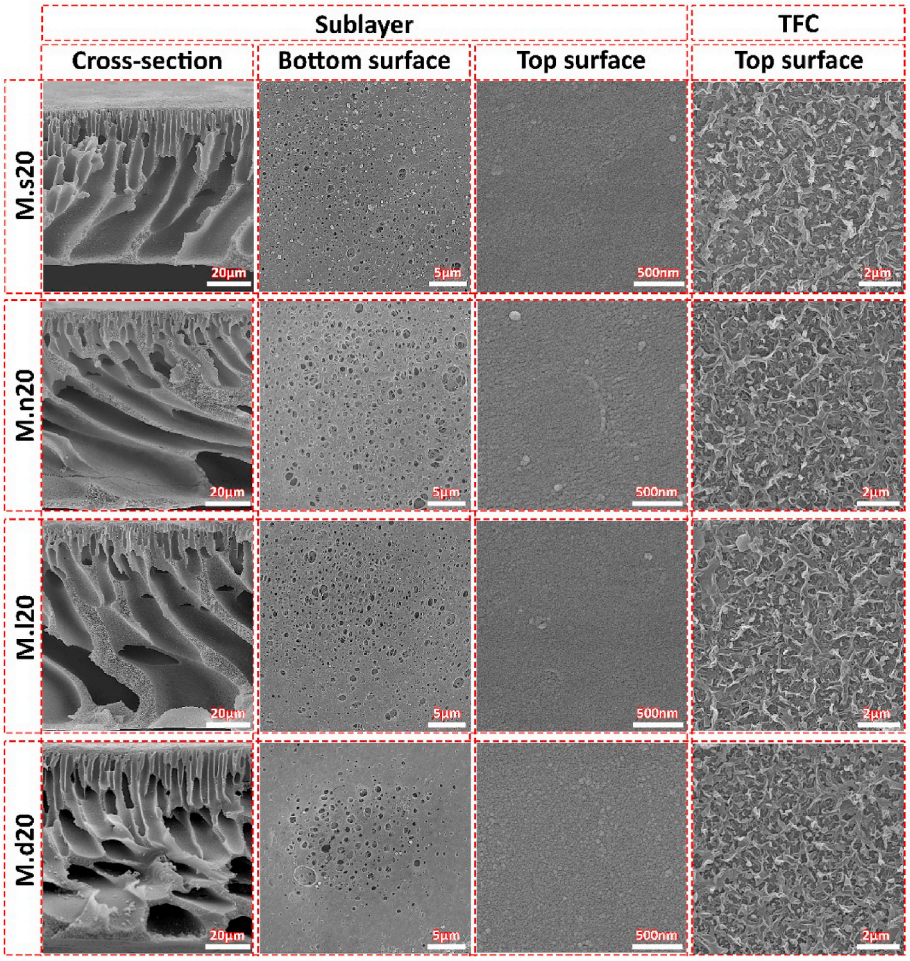

Fig. 2. Morphology of substrate and TFC membrane modified with different graft copolymer.

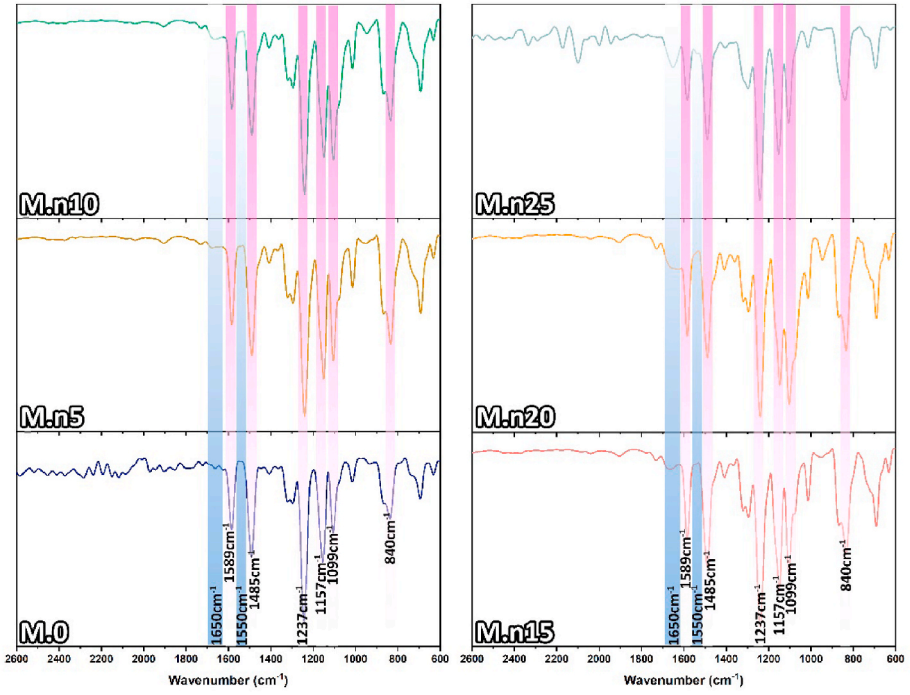

Fig. 3. FTIR analysis of control and modified substrates.

Table 4
Characteristics of sublayers with different loading of the graft copolymer.

Substarte	WCA (°)	Porosity (%)	PWP (LMH/bar)	Pore size (nm)
M.0	80.1 ± 1.7	77.3 ± 1.2	79.7 ± 11.9	13.7
M.n5	78.2 ± 1.1	80.5 ± 1.2	133.4 ± 14.6	17.1
M.n10	75.9 ± 0.7	81.3 ± 0.6	203.5 ± 13.1	21.2
M.n15	72.4 ± 1.2	82.5 ± 1.3	286.1 ± 20.2	24.8
M.n20	69.3 ± 1.3	84.1 ± 0.2	345.3 ± 14.6	26.9
M.n25	64.1 ± 1.7	80.8 ± 1.4	326.8 ± 13.9	26.1

On the contrary, the PWP of the M.n20 sublayer rises from 345.3 to 431.5 LMH/bar, with temperature increasing from 25 to 40 °C. This temperature-dependent water permeability is typical of a PNIPM brush-coated porous membrane. With an LCST of ~32 °C, PNIPM is stretched at lower temperatures leading to pore size decline, reducing the water permeability of the membrane [36]. At 40 °C, the PNIPM side chains shrink and present a more hydrophobic surface on the pore and membrane. Consequently, the mean pore size and the water permeability through the sublayer are raised [37]. This behavior is schematically depicted in Fig. 4a. To investigate the reversibility and stability of the copolymer blended sublayer during separation process, the temperature dependent PWP of the modified sublayer is measured at 25 °C and 40 °C (Fig. 4b). During five cycles of the PWP test, the M.n20 sublayer shows a reversible flux change at 25 and 40 °C.

The prepared sublayer morphologies were studied using SEM images to evaluate the sublayers' structure after the blending with the copolymer. As shown in Fig. 5, all sublayers have typical asymmetric morphologies with a denser top-layer and a porous sub-layer. Upon blending PSf-g-PNIPM copolymer into the sublayer matrix, some variations occur on the modified sublayers' cross-section morphology. The control PSf has a partial sponge-like structure, while the modified sublayers possess a full finger-like morphology. With increasing mass ratio of graft copolymer from 0 to 20 wt%, the finger-like pores become more apparent and interconnected with each other. The change in sublayer morphology is mainly due to the presence of graft copolymer in the polymer dope solution, which leads to a decreased exchange rate between solvent and non-solvent during phase inversion [31]. The increased affinity of the PNIPM containing blend to water compared to control PSf leads to a slower exchange rate, which results in larger finger-like morphology [38].

The top and bottom surface morphologies of the sublayers after the copolymer blending are shown in Fig. 6. The number of pores and overall porosity of the bottom surface rise with increasing PSf-g-PNIPM content from 0 to 20 wt%. The variation in morphology could be attributed to the following factors: (1) the affinity of the glass plate to the casting solution and (2) the time between the onset of gelation and film floating [39]. In general, a bottom surface with large pores and porosity could facilitate the water and salt diffusion into the sublayer to reduce the ICP effect. A smooth and defect-free top surface was observed for all substrates, unlike the bottom surfaces. This morphology is suitable for the formation of a defect-free PA thin film via IP procedure.

Characteristics and performances of the TFC membranes. A dense and selective PA thin film on top of the porous sublayer is fundamentally key to obtain a high water flux and selectivity as to prevent draw agent losses in FO processes. To explore the effect of graft copolymer content on the PA thin film morphology, SEM analysis was performed and shown in Fig. 7. According to the top surface images, a ridge-and-valley morphology as the typical IP reaction morphology between MPD and TMC was found for all TFC membranes. The incorporation of graft copolymer into the sublayer matrix regardless of its concentration, lead to some changes in the PA layer morphology. The ridge structure's size and numbers in the modified membranes increase with the graft copolymer weight ratio. The PA film thickness was also evaluated using cross-section SEM images. Based on these images, thicker PA layers were observed as the PSf-g-PNIPM blend ratio increased. Hoek's conceptual model of the PA thin film formation mechanism may explain the thickness and roughness of the PA thin films formed on the modified sublayers [40]. Based on this model, the IP process starts growing by diffusion of MPD molecules from the saturated sublayer pores to the organic side. Therefore, the IP reaction mostly occurs on the organic side. The substrate's hydrophilicity and pore size play a vital role in the diffusion of MPD, and, consequently, the PA thin film's overall characteristics. The large pores of the modified sublayer facilitate MPD diffusion, resulting in a more rough and thick PA thin film [27]. The neat PSf sublayer with smaller pores supports the formation of a thin and smooth PA layer [41].

AFM was conducted to confirm the surface morphology differences. Fig. 8 shows the AFM images and mean roughness (R_a) of the different composite membranes. The roughness trend from the neat TFC membrane to the TFC-n25 membrane is supports the visual observation from SEM.

Separation Properties. TFC membranes with different mass ratios

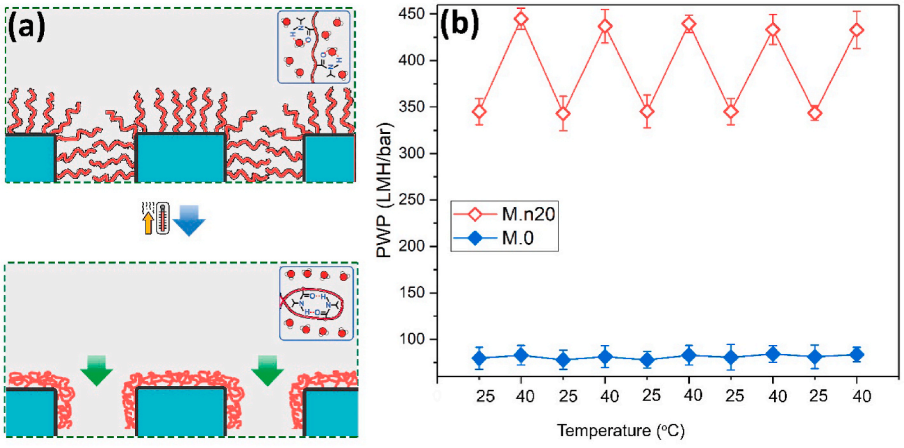

Fig. 4. (a) Illustration of the switching mechanism for the PNIPM containing blend substrate and (b) reversabilty test of M.n20 substrate.

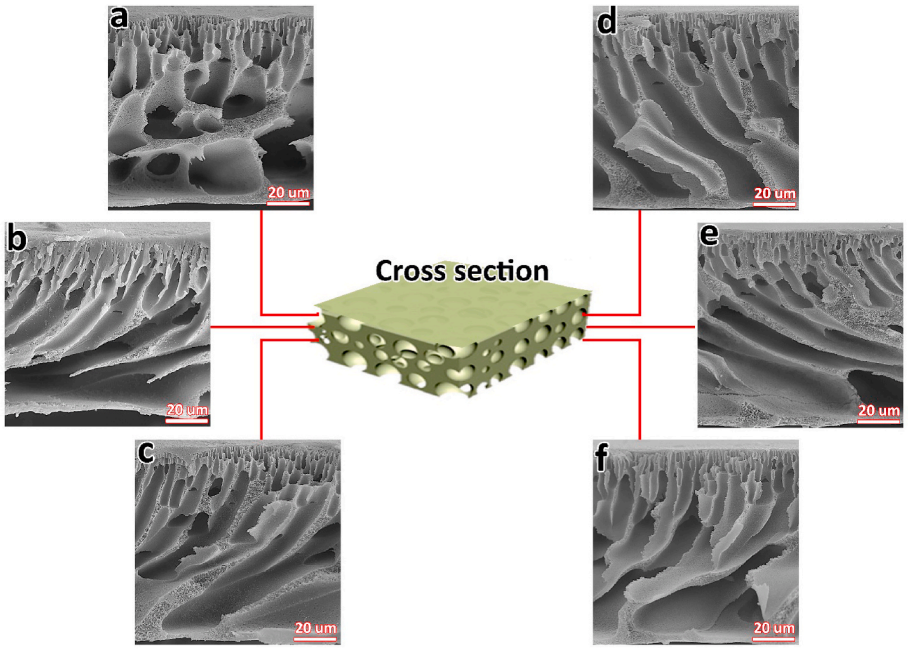

Fig. 5. SEM images of control and modified sublayers (a) M.0, (b) M.n5, (c) M.n10, (d) M.n15, (e) M.n20, and (f) M.n25.

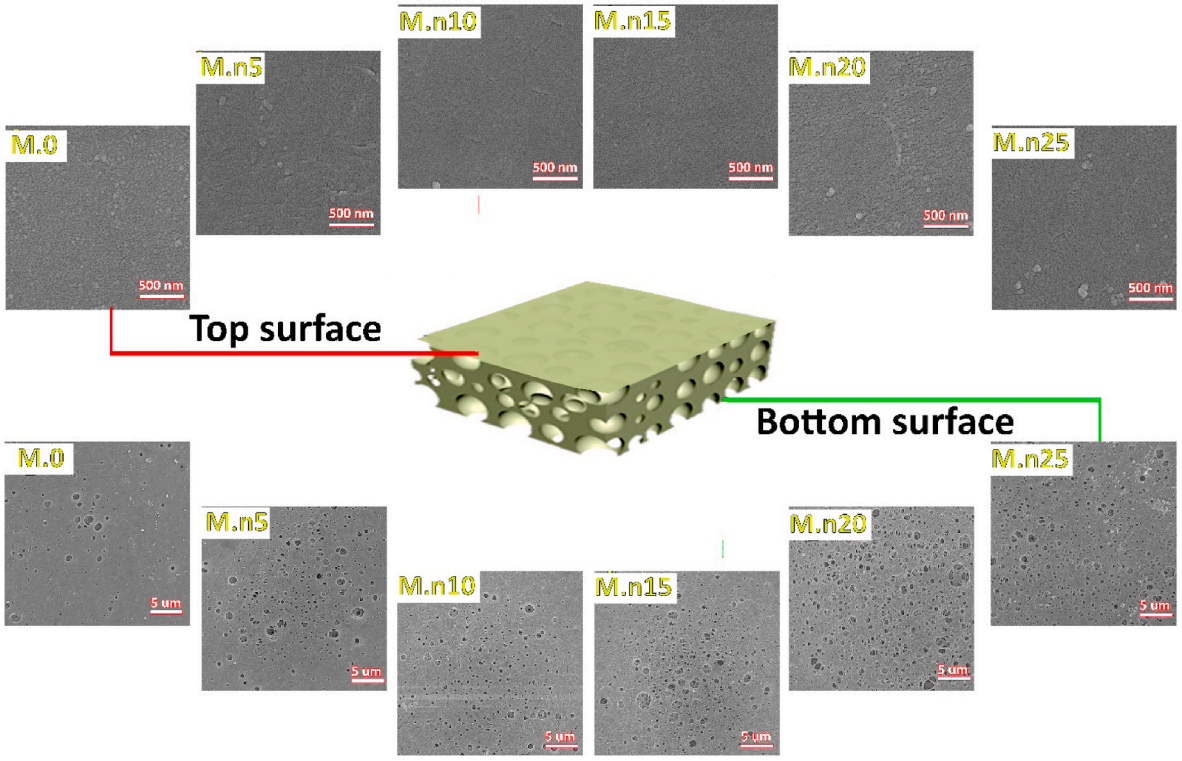

Fig. 6. Top and bottom surface SEM images of sublayers.

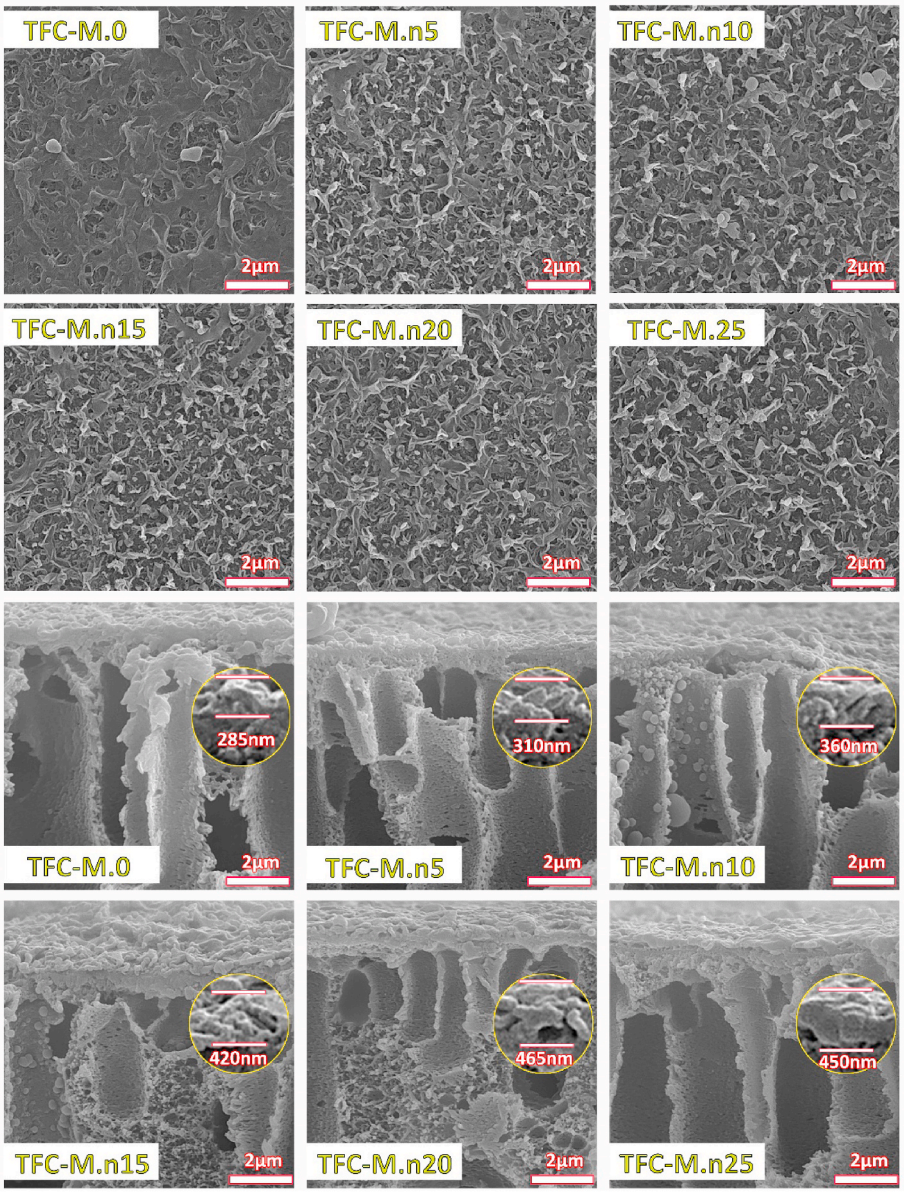

Fig. 7. Top and cross-section SEM images of TFC membranes.

of PSf-g-PNIPM were further investigated in RO process. The results, including A, B and R_s are summarized in Table 5. A general increase in A and B is observed when the graft copolymer blend ratio is raised in the sublayer matrix. The increase in A may be due to the rougher PA thin film with a larger surface area for water permeance [42]. The B value increase follows an intrinsic permeability-selectivity trade-off in which raising A comes with an even bigger B [43]. Moreover, the salt rejection confirmed a uniform and defect-free structure with an equal or higher R_s value compared to the control TFC membrane. The higher salt rejection in the modified membranes may be caused by high adsorption and uniform dispersion of the MPD solution on the hydrophilic PSf/PSf-g-PNIPM sublayer. Therefore, there are too high available MPD to react with TMC monomers, resulting in a uniform and selective PA layer [44].

FO performance. Fig. 9 illustrates the water flux, reverse salt flux, and selectivity for TFC membranes with different sublayers determined in the FO mode using DI water and 1 M NaCl as feed and draw solution, respectively. In general, both the dense PA thin-film and the porous sublayer determine the water flux of TFC membranes in the FO process [45]. Therefore, the variations of water flux in the modified TFC membranes are consistent with the difference in their sublayer and PA thin-film physicochemical characteristics, as shown in Figs. 5–7. In other words, the higher water flux of the modified TFC membranes, as shown in Fig. 9 may be ascribed to the following parameter: (1) a rougher PA thin-film tends to improve the water flux by providing a large transport area for water, (2) finger-like morphology tend to enhance the water flux by increasing draw agent diffusion into the substrate pore and (3) the proper rise of the sublayer hydrophilicity and porosity usually can improve the water flux [6,46]. In addition, the reverse salt flux shows a similar trend as that seen for the R_s parameter in RO. The PA thin-film largely determines the reverse salt flux of the TFC membranes. The lower reverse salt flux in the TFC membranes with modified sublayers may be caused by the uniform dispersion of the MPD solution on the hydrophilic PSf/PSf-g-PNIPM sublayers and consequently a more homogeneous PA thin film. The J_s/J_w ratio (selectivity) was measured to evaluate the performance and efficiency of different TFC-FO membranes. A high-performance FO membrane needs a low reverse salt flux and high water flux (low J_s/J_w ratio) [42,47]. With increasing mass ratio of the graft copolymer in the sublayer, the resulting TFC membrane's selectivity significantly improved, with the lowest J_s/J_w ratio of 0.07

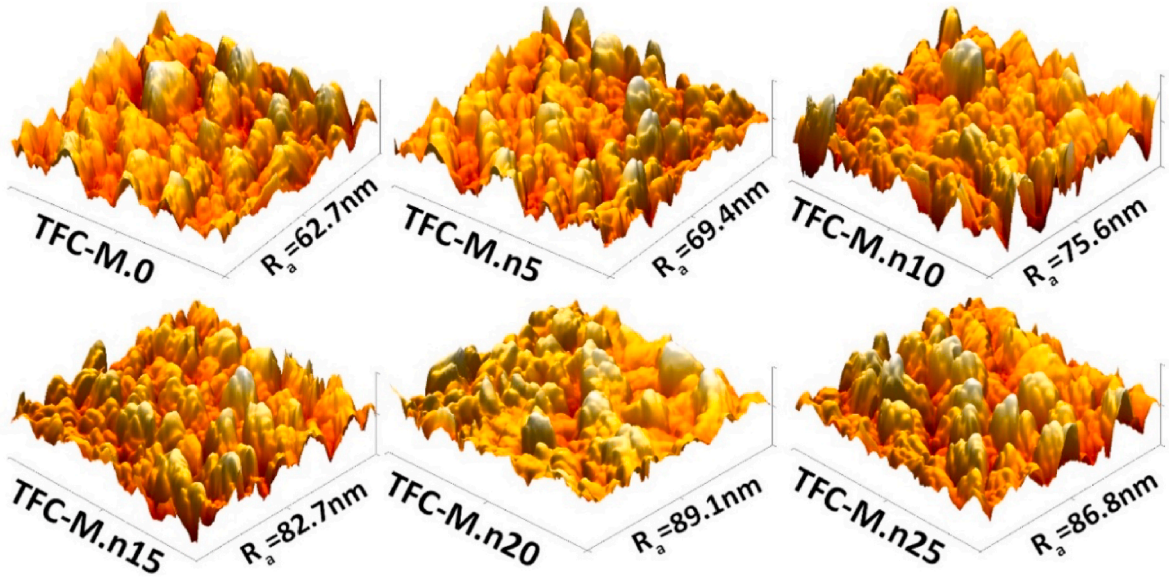

Fig. 8. 3D AFM images of different TFC membranes. Mean roughness values are indicated.

Table 5
RO performance of composite membrane.

Membrane	A (LMH/bar)	R_s (%)	B (LMH)	S (μm)
TFC-M.0	1.21 ± 0.11	94.31 ± 0.31	0.34 ± 0.04	1915 ± 137
TFC-M.n5	1.81 ± 0.13	95.21 ± 0.30	0.45 ± 0.05	693 ± 109
TFC-M.n10	2.11 ± 0.16	95.56 ± 0.52	0.49 ± 0.07	546 ± 77
TFC-M.n15	2.29 ± 0.06	95.92 ± 0.53	0.49 ± 0.08	418 ± 31
TFC-M.n20	2.71 ± 0.05	94.57 ± 0.35	0.78 ± 0.04	272 ± 19
TFC-M.n25	2.66 ± 0.11	94.37 ± 0.45	0.76 ± 0.05	305 ± 15

g/L achieved for TFC-nM15.

To assess the ICP effect in substrates, the S parameter, a typical metric of ICP, was calculated from the RO and FO data [48]. Due to their suitable morphology and characteristics, the modified membranes showed a lower S value than the control membrane. This means a lower ICP for the TFC membranes with a porous sublayer. These findings suggest that the PSf/PSf-g-PNIPM blend has great merit for use as the sublayer of high-performance TFC-FO membranes.

Temperature dependent morphology. Due to the thermoresponsive behavior of PSf-g-PNIPM, the non-solvent temperature (n-ST) affects the phase inversion process of the sublayer. Before studying the impact of the n-ST on the membranes' characteristics and performance, it is necessary to understand the phase inversion mechanism of the amphiphilic graft copolymer. NMP is a good solvent for both the PNIPM and PSf segments. Upon immersing the casted membrane in non-solvent, the PSf segments associate hydrophobically and precipitate out from the aqueous medium, while the hydrophilic PNIPM segments remain fully stretched. The strong incompatibility of the PSf and PNIPM segments induce the graft copolymer to experience phase inversion. Since the water is a good solvent for the PNIPM segments, plenty of water is trapped inside the hydrophilic PNIPM chains' hydrodynamic volume. After drying, the hydrophilic PNIPM segments shrink and coat the PSf surfaces with hydrophilic grafts [49]. Any variation in the n-ST is likely to change the hydrophilicity of PNIPM segments, which subsequently changes the sublayers' performance and final morphology.

With the increase in n-ST from 25 to 40 °C, as shown in Table 6, the porosity of the resulted M.nh20 sublayer decreases from 84.1 to 81.8%. The PWP decreases correspondingly from 345 to 285 LMH/bar. Besides, the FO water flux of the TFC-M.nh20 is lower than the TFC-M.n20. It is caused by the lower porosity and hydrophilicity of the M.nh20 sublayer formed in non-solvent at high temperature. In comparison to the M.n20 sublayer, the M.nh20 sublayer has shorter macro voids lengths and narrower sizes. Therefore, the M.nh20 sublayer has a larger S parameter,

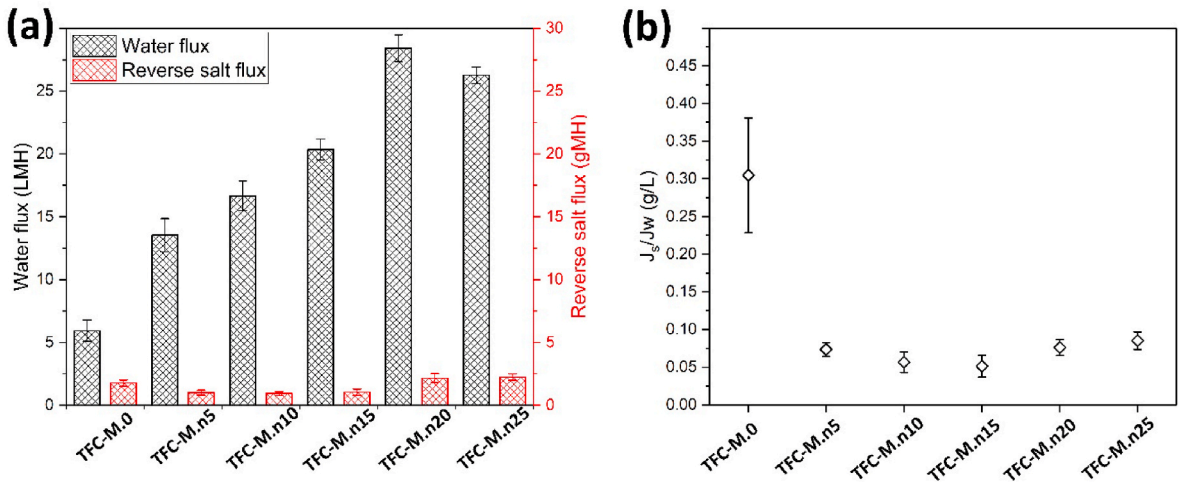

Fig. 9. (a) water and reverse salt fluxes and (b) selectivity of different composite membranes in FO mode.

Table 6
Characteristics and performance of M.nh20 substrate and TFC-M.nh20 membrane.

Membrane	Substrate				Membrane	TFC	
	Porosity (%)	WCA (°)	PWP (LMH/bar)	Pore size (nm)		J_w (LMH)	J_s (gMH)
M.nh20	81.8 ± 0.4	71.9 ± 0.6	285.3 ± 11.4	24.6	TFC-M.h20	22.2 ± 0.7	1.9 ± 0.18

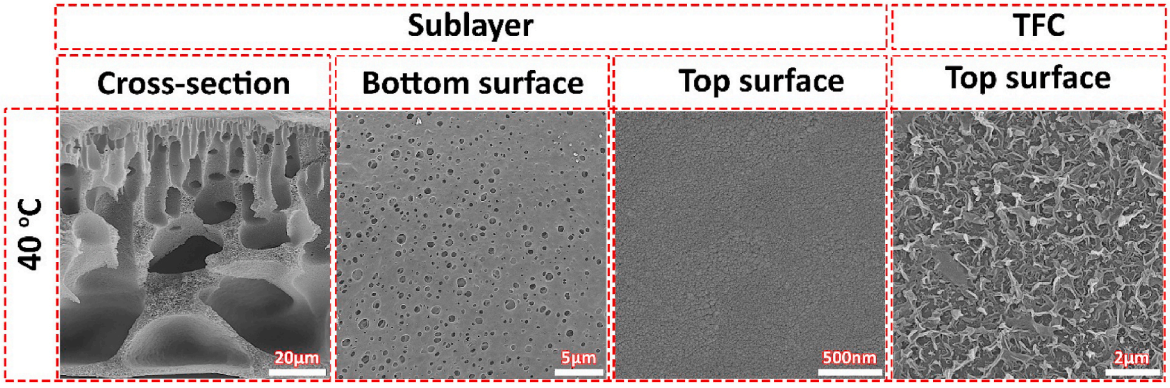

Fig. 10. SEM images of M.nh20 sublayer and TFC-M.nh20 membrane.

resulting in a more severe ICP and a lower water flux in the TFC-M.nh20. These results are consistent with the PNIPM side chains' hydrophobic association near and above the LCST at the water-solvent interface and on the membrane surface. Based on the proposed mechanism for phase inversion of amphiphilic graft copolymer, below the LCST the PNIPM segments assume a hydrophilic state with a fully extended structure, giving rise to larger pore sizes. Above the LCST, the PNIPM segments assume a hydrophobic state with a collapsed structure, leading to a decline in porosity and pore size of the resulting M.nh20 sublayer (see Fig. 10). The proposed mechanism is also in-line with the fact that the hydrophilicity of the M.n20 is higher than that of the M.nh20. This could be attributed to the PNIPM segments' migration to the membrane surface during phase inversion, as PNIPM assumes a hydrophilic structure at low temperatures.

4. Conclusion

In this research, a highly porous, hydrophilic, and water permeable substrate was fabricated using PSf as the main membrane polymer and PSf-g-PNIPM graft copolymer as the amphiphilic additive. The copolymer was introduced into the sublayer matrix to improve the water flux of the fabricated TFC-FO membrane and decrease its S parameter by taking advantage of the morphology, low tortuosity, high porosity and hydrophilicity of the modified sublayers. The PSf-g-PNIPM modified support layer reveals temperature dependent permeability for aqueous solutions. In addition, the temperature of the non-solvent during phase inversion can be used to control the morphology and performance of the support layer. In the FO process, the copolymer modified TFC membranes presented a superior performance with a highest water flux of 28.4 LMH for the TFC-M.n20 membrane. The FO performance test shows that the copolymer modified sublayer provided a smooth and hydrophilic surface for IP reaction to form a defect-free and uniform PA thin film with very high selectivity. This study's results highlight the promising potential of PSf-g-PNIPM copolymer in the fabrication of thermoresponsive sublayers for TFC membranes and demonstrate valuable guidance to optimize the permselectivity of PA thin films in the TFC-FO membranes.

Notes

The authors declare no competing financial interest.

Author agreement statement

We the undersigned declare that this manuscript is original, has not been published before and is not currently being considered for publication elsewhere.

We confirm that the manuscript has been read and approved by all named authors and that there are no other persons who satisfied the criteria for authorship but are not listed.

We further confirm that the order of authors listed in the manuscript has been approved by all of us.

We understand that the Corresponding Author is the sole contact for the Editorial process.He/she is responsible for communicating with the other authors about progress, submissions of revisions and final approval of proofs Signed by all authors as follows:

Declaration of competing interest

The authors declare that they have no known competing financial interests or personal relationships that could have appeared to influence the work reported in this paper.

Data availability

No data was used for the research described in the article.

Acknowledgments

The authors gratefully acknowledge the financial support of the University of Tehran.

Appendix A. Supplementary data

Supplementary data to this article can be found online at https://doi.org/10.1016/j.memsci.2022.120794.

References

[1] B.E. Logan, M. Elimelech, Membrane-based processes for sustainable power generation using water, Nature 488 (2012) 313–319, https://doi.org/10.1038/nature11477.

[2] S. Qi, Y. Li, Y. Zhao, W. Li, C.Y. Tang, Highly efficient forward osmosis based on porous membranes-Applications and implications, Environ. Sci. Technol. 49 (2015) 4690–4695, https://doi.org/10.1021/es504164w.

[3] Y. Shi, X. Liao, R. Chen, Q. Ge, pH-Responsive polyoxometalates that achieve efficient wastewater reclamation and source recovery via forward osmosis, Environ. Sci. Technol. 55 (2021) 12664–12671, https://doi.org/10.1021/acs.est.1c04245.

[4] A. Shakeri, H. Salehi, S.R. Razavi, S.M. Mirahmadi Babaheydari, Blue lemon@ quaternary graphene oxide open frameworks: as a novel nanostructure for performance enhancement of thin film nanocomposite forward osmosis membrane, Chem. Eng. Res. Des. 148 (2019) 451–459, https://doi.org/10.1016/j.cherd.2019.06.035.

[5] K. Zheng, S. Zhou, X. Zhou, A low-cost and high-performance thin-film composite forward osmosis membrane based on an SPSU/PVC substrate, Sci. Rep. 8 (2018), 10022, https://doi.org/10.1038/s41598-018-28436-4.

[6] Y. Zhao, X. Wang, Y. Ren, D. Pei, Mesh-Embedded polysulfone/sulfonated polysulfone supported thin film composite membranes for forward osmosis, ACS Appl. Mater. Interfaces 10 (2018) 2918–2928, https://doi.org/10.1021/acsami.7b15309.

[7] P.F. Sun, Z. Yang, X. Song, J.H. Lee, C.Y. Tang, H.D. Park, Interlayered forward osmosis membranes with Ti3C2TxMXene and carbon nanotubes for enhanced municipal wastewater concentration, Environ. Sci. Technol. 55 (2021) 13219–13230, https://doi.org/10.1021/acs.est.1c01968.

[8] M. Son, T. Kim, W. Yang, C.A. Gorski, B.E. Logan, Electro-forward osmosis, Environ. Sci. Technol. 53 (2019) 8352–8361, https://doi.org/10.1021/acs.est.9b01481.

[9] N.N. Bui, J.R. McCutcheon, Nanoparticle-embedded nanofibers in highly permselective thin-film nanocomposite membranes for forward osmosis, J. Membr. Sci. 518 (2016) 338–346, https://doi.org/10.1016/j.memsci.2016.06.024.

[10] D.L. Shaffer, J.R. Werber, H. Jaramillo, S. Lin, M. Elimelech, Forward osmosis: where are we now? Desalination 356 (2015) 271–284, https://doi.org/10.1016/j.desal.2014.10.031.

[11] S. Sahebi, S. Phuntsho, Y.C. Woo, M.J. Park, L.D. Tijing, S. Hong, H.K. Shon, Effect of sulphonated polyethersulfone substrate for thin film composite forward osmosis membrane, Desalination 389 (2016) 129–136, https://doi.org/10.1016/j.desal.2015.11.028.

[12] Z. Zhou, J.Y. Lee, T.S. Chung, Thin film composite forward-osmosis membranes with enhanced internal osmotic pressure for internal concentration polarization reduction, Chem. Eng. J. 249 (2014) 236–245, https://doi.org/10.1016/j.cej.2014.03.049.

[13] D. Emadzadeh, W.J. Lau, T. Matsuura, M. Rahbari-Sisakht, A.F. Ismail, A novel thin film composite forward osmosis membrane prepared from PSf-TiO2 nanocomposite substrate for water desalination, Chem. Eng. J. 237 (2014) 70–80, https://doi.org/10.1016/j.cej.2013.09.081.

[14] J. Ren, B. O'Grady, G. deJesus, J.R. McCutcheon, Sulfonated polysulfone supported high performance thin film composite membranes for forward osmosis, Polym. (United Kingdom). 103 (2016) 486–497, https://doi.org/10.1016/j.polymer.2016.02.058.

[15] R. Ghalavand, M. Mokhtary, A. Shakeri, O. Alizadeh, ZnO@PMMA incorporated PSf substrate for improving thin-film composite membrane performance in forward osmosis process, Chem. Eng. Res. Des. 177 (2022) 594–603, https://doi.org/10.1016/J.CHERD.2021.11.017.

[16] Z. Alihemati, S.A. Hashemifard, T. Matsuura, A.F. Ismail, On Performance and fouling of thin film composite hollow Fiber membranes using polycarbonate/polyvinylchloride as porous substrates for forward osmosis applications, J. Environ. Chem. Eng. 10 (2022), 106828, https://doi.org/10.1016/j.jece.2021.106828.

[17] J.J. Huang, X. Mei, J. Han, L. Yao, S. Chen, X. You, Y. Liao, Impacts of hydrophobic, hydrophilic, superhydrophobic and superhydrophilic nanofibrous substrates on the thin film composite forward osmosis membranes, J. Environ. Chem. Eng. 10 (2022), 106958, https://doi.org/10.1016/j.jece.2021.106958.

[18] M. Qiu, J. Wang, C. He, A stable and hydrophilic substrate for thin-film composite forward osmosis membrane revealed by in-situ cross-linked polymerization, Desalination 433 (2018) 1–9, https://doi.org/10.1016/j.desal.2018.01.021.

[19] K. Zheng, S. Zhou, X. Zhou, High-performance thin-film composite forward osmosis membrane fabricated on low-cost PVB/PVC substrate, New J. Chem. 42 (2018) 13382–13392, https://doi.org/10.1039/C8NJ01677A.

[20] P. Lu, W. Li, S. Yang, Y. Wei, Z. Zhang, Y. Li, Layered double hydroxides (LDHs) as novel macropore-templates: the importance of porous structures for forward osmosis desalination, J. Membr. Sci. 585 (2019) 175–183, https://doi.org/10.1016/j.memsci.2019.05.045.

[21] A.A. Shah, Y.H. Cho, H. Choi, S.-E. Nam, J.F. Kim, Y. Kim, Y.-I. Park, H. Park, Facile integration of halloysite nanotubes with bioadhesive as highly permeable interlayer in forward osmosis membranes, J. Ind. Eng. Chem. 73 (2019) 276–285, https://doi.org/10.1016/j.jiec.2019.01.039.

[22] T.M. Salehi, M. Peyravi, M. Jahanshahi, W.J. Lau, A.S. Rad, Impacts of zeolite nanoparticles on substrate properties of thin film nanocomposite membranes for engineered osmosis, J. Nanoparticle Res. 20 (2018), https://doi.org/10.1007/s11051-018-4154-1.

[23] Y. Yang, L. Miao, J. Hu, G. Liu, Y. Tu, S. Lin, F. Liu, F. Li, Y. Wu, G. Zhang, H. Zou, Hydrophilization of polysulfone membranes using a binary graft copolymer, J. Mater. Chem. A. 2 (2014) 10410–10423, https://doi.org/10.1039/C4TA01481B.

[24] Z. Yi, L.P. Zhu, Y.Y. Xu, Y.F. Zhao, X.T. Ma, B.K. Zhu, Polysulfone-based amphiphilic polymer for hydrophilicity and fouling-resistant modification of polyethersulfone membranes, J. Membr. Sci. 365 (2010) 25–33, https://doi.org/10.1016/j.memsci.2010.08.001.

[25] J.Y. Park, M.H. Acar, A. Akthakul, W. Kuhlman, A.M. Mayes, Polysulfone-graft-poly(ethylene glycol) graft copolymers for surface modification of polysulfone membranes, Biomaterials 27 (2006) 856–865, https://doi.org/10.1016/j.biomaterials.2005.07.010.

[26] Y.Q. Wang, Y.L. Su, Q. Sun, X. Le Ma, Z.Y. Jiang, Generation of anti-biofouling ultrafiltration membrane surface by blending novel branched amphiphilic polymers with polyethersulfone, J. Membr. Sci. 286 (2006) 228–236, https://doi.org/10.1016/j.memsci.2006.09.040.

[27] H. Salehi, A. Shakeri, H. Mahdavi, R.G.H. Lammertink, Improved performance of thin-film composite forward osmosis membrane with click modified polysulfone substrate, Desalination 496 (2020), 114731, https://doi.org/10.1016/j.desal.2020.114731.

[28] W. Ding, Y. Li, M. Bao, J. Zhang, C. Zhang, J. Lu, Highly permeable and stable forward osmosis (FO) membrane based on the incorporation of Al2O3 nanoparticles into both substrate and polyamide active layer, RSC Adv. 7 (2017) 40311–40320, https://doi.org/10.1039/C7RA04046F.

[29] Q. Shi, J.Q. Meng, R.S. Xu, X.L. Du, Y.F. Zhang, Synthesis of hydrophilic polysulfone membranes having antifouling and boron adsorption properties via blending with an amphiphilic graft glycopolymer, J. Membr. Sci. 444 (2013) 50–59, https://doi.org/10.1016/j.memsci.2013.05.014.

[30] S. Khoee, P. Mansouri Bakvand, Synthesis of dual-responsive Janus nanovehicle via PNIPAm modified SPIONs deposition on crosslinked chitosan microparticles and decrosslinking process in the core, Eur. Polym. J. 114 (2019) 411–425, https://doi.org/10.1016/j.eurpolymj.2019.03.007.

[31] A. Rahimpour, S.S. Madaeni, S. Ghorbani, A. Shockravi, Y. Mansourpanah, The influence of sulfonated polyethersulfone (SPES) on surface nano-morphology and performance of polyethersulfone (PES) membrane, Appl. Surf. Sci. 256 (2010) 1825–1831, https://doi.org/10.1016/j.apsusc.2009.10.014.

[32] J.F. Blanco, J. Sublet, Q.T. Nguyen, P. Schaetzel, Formation and morphology studies of different polysulfones-based membranes made by wet phase inversion process, J. Membr. Sci. 283 (2006) 27–37, https://doi.org/10.1016/j.memsci.2006.06.011.

[33] K. Mohanty, M.K. Purkait, Membrane Technologies and Applications, John Wiley & Sons, Ltd, Chichester, UK, 2011, https://doi.org/10.1002/0470020393.

[34] J.Z. Yu, L.P. Zhu, B.K. Zhu, Y.Y. Xu, Poly(N-isopropylacrylamide) grafted poly (vinylidene fluoride) copolymers for temperature-sensitive membranes, J. Membr. Sci. 366 (2011) 176–183, https://doi.org/10.1016/j.memsci.2010.09.055.

[35] Y. Zhu, S. Gao, L. Hu, J. Jin, Thermoresponsive ultrathin membranes with precisely tuned nanopores for high-flux separation, ACS Appl. Mater. Interfaces 8 (2016) 13607–13614, https://doi.org/10.1021/acsami.6b03389.

[36] B. Ma, X.J. Ju, F. Luo, Y.Q. Liu, Y. Wang, Z. Liu, W. Wang, R. Xie, L.Y. Chu, Facile fabrication of composite membranes with dual thermo- and pH-responsive characteristics, ACS Appl. Mater. Interfaces 9 (2017) 14409–14421, https://doi.org/10.1021/acsami.7b02427.

[37] T. Cai, K.G. Neoh, E.T. Kang, Surface-functionalized and surface-functionalizable poly (vinylidene fluoride) graft copolymer membranes via click chemistry and atom transfer radical polymerization, Langmuir 27 (2011) 2936–2945, https://doi.org/10.1021/la2001514.

[38] X. Zhang, L. Shen, W.-Z. Lang, Y. Wang, Improved performance of thin-film composite membrane with PVDF/PFSA substrate for forward osmosis process, J. Membr. Sci. 535 (2017) 188–199, https://doi.org/10.1016/j.memsci.2017.04.038.

[39] M. Corvilain, C. Klaysom, A. Szymczyk, I.F.J. Vankelecom, Formation mechanism of sPEEK hydrophilized PES supports for forward osmosis, Desalination 419 (2017) 29–38, https://doi.org/10.1016/J.DESAL.2017.05.037.

[40] A.K. Ghosh, E.M.V. V Hoek, Impacts of support membrane structure and chemistry on polyamide-polysulfone interfacial composite membranes, J. Membr. Sci. 336 (2009) 140–148, https://doi.org/10.1016/j.memsci.2009.03.024.

[41] X. Li, K.Y. Wang, B. Helmer, T.S. Chung, Thin-film composite membranes and formation mechanism of thin-film layers on hydrophilic cellulose acetate propionate substrates for forward osmosis processes, Ind. Eng. Chem. Res. 51 (2012) 10039–10050, https://doi.org/10.1021/ie2027052.

[42] S.F. Seyedpour, M.D. Firouzjaei, A. Rahimpour, E. Zolghadr, A.A. Shamsabadi, P. Das, F.A. Afkhami, M. Sadrzadeh, A. Tiraferri, M. Elliott, Toward sustainable tackling of biofouling implications and improved performance of TFC FO membranes modified by Ag-MOF nanorods, ACS Appl. Mater. Interfaces 12 (2020) 38285–38298, https://doi.org/10.1021/ACSAMI.0C13029.

[43] M. Rastgar, A. Bozorg, A. Shakeri, Novel dimensionally controlled nanopore forming template in forward osmosis membranes, Environ. Sci. Technol. 52 (2018) 2704–2716, https://doi.org/10.1021/acs.est.7b05583.

[44] X. Zhang, Y. Zeng, C. Shen, Z. Fan, Q. Meng, W. Zhang, G. Zhang, C. Gao, In situ assembly of polyamide/fe(btc) nanocomposite reverse osmosis membrane assisted by fe3+-polyphenolic complex for desalination, ACS Appl. Mater. Interfaces 13 (2021) 48679–48690, https://doi.org/10.1021/acsami.1c13801.

[45] A. Shakeri, S.M.M. Babaheydari, H. Salehi, S.R. Razavi, Reduction of the structure parameter of forward osmosis membranes by using sodium bicarbonate as pore-forming agent, Langmuir 37 (2021) 7591–7599, https://doi.org/10.1021/acs.langmuir.1c01097.

[46] P.H.H. Duong, S. Chisca, P.Y. Hong, H. Cheng, S.P. Nunes, T.S. Chung, Hydroxyl functionalized polytriazole-co-polyoxadiazole as substrates for forward osmosis membranes, ACS Appl. Mater. Interfaces 7 (2015) 3960–3973, https://doi.org/10.1021/am508387d.

[47] Q. Saren, C.Q. Qiu, C.Y. Tang, Synthesis and characterization of novel forward osmosis membranes based on layer-by-layer assembly, Environ. Sci. Technol. 45 (2011) 5201–5208, https://doi.org/10.1021/es200115w.

[48] A. Deshmukh, N.Y. Yip, S. Lin, M. Elimelech, Desalination by forward osmosis: identifying performance limiting parameters through module-scale modeling, J. Membr. Sci. 491 (2015) 159–167, https://doi.org/10.1016/j.memsci.2015.03.080.

[49] J. Xue, L. Chen, H.L. Wang, Z.B. Zhang, X.L. Zhu, E.T. Kang, K.G. Neoh, Stimuli-Responsive multifunctional membranes of controllable morphology from poly (vinylidene fluoride)- *graft* -Poly[2-(*N,N* -dimethylamino)ethyl methacrylate] prepared via atom transfer radical polymerization, Langmuir 24 (2008) 14151–14158, https://doi.org/10.1021/la801402u.